

## A Scandium Modified Al-0.7 Fe Binary Alloy: Improvement of Creep-Resistance Property

Jiayi Zhang<sup>1</sup>, Xinyang Jiang<sup>1</sup>, Mingyang Ma<sup>1</sup>, Bin Wang<sup>1,2\*</sup>, Danqing Yi<sup>1,2</sup> and Bo Jiang<sup>1</sup><sup>1</sup>School of Material Science and Engineering, Central South University, Changsha 410083, PR China<sup>2</sup>Light Alloy Research Institute, Central South University, Changsha 410083, PR China

### Abstract

The creep behaviors and microstructures of Al-0.7Fe and Al-0.7Fe-0.2Sc alloy are investigated through creep tests, optical microscope, electron probe micro-analyze and transmission electron microscope observations. It is found that the steady state creep rates of Al-0.7Fe-0.2Sc are smaller than that of Al-0.7Fe under different temperatures at 70 Mpa. An overview of microstructure is given, the interactions between intermetallic phases and dislocations are investigated, with an emphasis on the Al<sub>3</sub>Sc precipitates. The mechanism controlling creep-resistance is explained by Orowan strengthening mechanism. The magnitude of  $\Delta\sigma_{Or}$  can afford dislocations to bypass Al<sub>3</sub>Sc precipitates in Al-0.7Fe-0.2Sc alloy. The counter flow of the vacancies and solute atoms are induced to expound the dislocation motion mechanism.

**Keywords:** Al-0.7Fe binary alloy; Creep behaviors; Al<sub>3</sub>Sc precipitates; Orowan strengthening mechanism; A counter flux

### Introduction

More recently, all aluminum alloy conductors (AAAC) have been widely used instead of steel-cored aluminum strand (ACSR) [1-3]. Such as AA8xxx aluminum alloy cables, which possess excellent mechanical properties, especially for its creep property [4]. Fe and Re are important alloying elements to 8xxx alloy cables, they can form the reinforced Al<sub>3</sub>Fe or Al<sub>3</sub>Re phase to enhance tensile strength and creep resistance of 8xxx alloy. Prospective applications of such alloy cables as structural materials imply a necessity to ameliorate their creep property, which can be obtained by several methods [5,6]. Without sacrificing the electrical conductivity excessively, an especially effective method is based on precipitation strengthening with the addition of metal elements with a low solubility in the matrix, such as Sc, Zr and Er [7-10]. Therefore, the micro-alloying addition of Sc with a low solution (the maximum solubility of 0.23 at % Sc at the eutectic temperature) in Al-Fe alloy may be of the interest.

Sc is a promising rare-earth as a ternary alloying element to Al-Fe alloys. Al<sub>3</sub>Sc precipitates have a high creep resistance property, since its sluggish diffusivity, formation of fine and coherent Al<sub>3</sub>Sc precipitates with the L1<sub>2</sub> structure [11,12]. Researchers have reported that the additions of Sc and Zr can impede decomposition of supersaturated solid solutions and slow down precipitate phase coarsening. Marsha et al. [13] investigated the forming Al<sub>3</sub>(Sc<sub>1-x</sub>Ti<sub>x</sub>) precipitates remain nanosize ~10 nm, when addition of 0.06% Sc into Al-Ti alloy. They found that precipitates provide outstanding creep resistance to Al-Sc-Ti alloy in the temperature range of 300°C to 425°C, the climb bypass by dislocations of the precipitates by creep stress from 17 Mpa to 7 Mpa. Some researchers have reported the formation of a core-shell structure precipitate with a core of Al<sub>3</sub>Er and the shell of Sc-enriched in Al-Sc-Er, due to the more sluggish diffusivity of Sc than Er [10,11,14]. Dalen et al. [15] reported that diffusivities of Er and Yb elements at 300°C are determined by calculating kinetics of precipitation, are fourfold and tenfold greater than Sc in Al substrate, respectively. Sc provides a more significant improvement in the creep resistance property, compared with Er and Yb.

The Al-based immiscible systems, such as Al-Fe, the main disadvantages of the as-cast Al-Fe alloys typically show the low mechanical strength. Cubero et al. [16] studied that the ultimate tensile strength of Al-2%Fe only reaches 120 Mpa. However, a dilute alloying element in the Al matrix cannot reduce significantly the

electrical conductivity. Moreover, finely dispersed intermetallic phases may improve creep resistance, tensile strength and thermal stability [17]. However, Sc modification improvement of the deformation Al-Fe binary alloy has not been discussed extensively. In this study, two alloys without and with Sc addition were compared in the present investigation. The aim of the present paper is to study the influence of the Sc addition on tension creep of deformation Al-0.7Fe alloys at experimental conditions 90°C to 150°C, 70 Mpa.

### Material and Methods

#### Materials

The alloys studied in the work were prepared using commercial pure aluminum (99.7%), master alloys of Al-20%Fe and Al-5%Sc (mass fraction). They were used as a raw material to produce Al-0.7%Fe and Al-0.7%Fe to 0.2%Sc. Pure Al was melted in a furnace at 760°C, and then according to the elements of two alloys, Fe and Sc were added into the Al melts, respectively. After melting, two alloys were cast into ingots

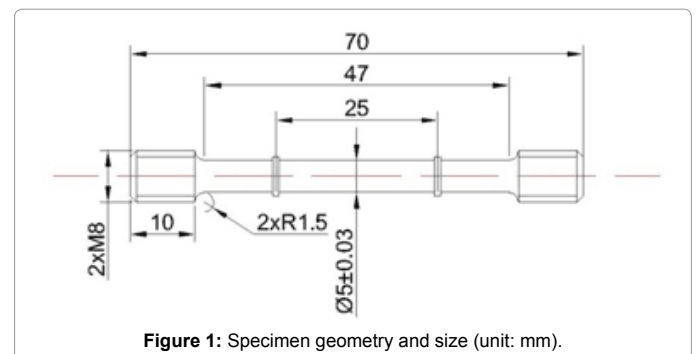


Figure 1: Specimen geometry and size (unit: mm).

\*Corresponding author: Bin Wang, School of Material Science and Engineering, Central South University, Changsha 410083, PR China, Tel: +86 731 88836320; E-mail: wangbin325@263.net

Received February 25, 2017; Accepted March 06, 2017; Published March 12, 2017

Citation: Zhang J, Jiang X, Ma M, Wang B, Yi D, et al. (2017) A Scandium Modified Al-0.7 Fe Binary Alloy: Improvement of Creep-Resistance Property. J Civil Environ Eng 7: 269. doi: 10.4172/2165-784X.1000269

Copyright: © 2017 Zhang J, et al. This is an open-access article distributed under the terms of the Creative Commons Attribution License, which permits unrestricted use, distribution, and reproduction in any medium, provided the original author and source are credited.

( $\Phi 50$  mm  $\times$  200 mm) by iron mold. All samples were homogenized heat at 500°C for 12h in air furnace, then extruded to wires of  $\Phi 10$  mm.

### Creep tests

The geometry of creep testing sample is shown in Figure 1. The tension creep tests were carried out in a SUST-D5 creep testing machine with an assisting furnace. The accuracies of temperature and loading system in tension creep testing machine are 0.1°C and 0.01 Mpa, respectively. In creep tests, the sample was performed in the furnace. The assisting furnace was divided into three thermocouples, which were tied in the top, middle and bottom specimen hot transfer rod. The displacement was measured with a linear variable differential transducer by attached an extensometer which was attached to the measure section of sample. The constant load creep tests were conducted for 100h, under the temperature of 90°C, 120°C and 150°C at 70 Mpa, respectively. After creep tests, the loading was released and the samples were cooled down to the room temperature. Additionally, tensile strength and yield strength were measured before and after creep tests at room temperature (5 mm/min strain rate).

### Characterization

The samples of two alloys were machined into cylinder samples  $\Phi 10$  mm  $\times$  10 mm, and the surfaces of the samples used for observation were polished and etched by Keller (95%wt H<sub>2</sub>O+2.5% wt HNO<sub>3</sub>+1.5% wt HCl+1.0% wt HF) alcohol solution. The metallurgical microstructures of these samples were examined by a optical microscope (OM) and a electron probe micro-analyze (EPMA).

Transmission electron microscope (TEM) specimens were cut perpendicularly to the applied stress direction from the creep testing samples. 1 mm thick disks of 5 mm in diameter were cut by wire cutting, and mechanically polished down to thick disks of about 70  $\mu$ m. The final thinning was prepared by twin-jet electro-polishing in a mixture solution of 25% nitric acid and 75% methanol (vol %) at about -25°C and 15 V. Microstructures were characterized by operating a Tecnai G<sup>2</sup> F20 transmission electron microscopy (TEM) at 200 kV. Additionally, TEM micrographs were used to measure the size of about 100 precipitates, and calculate the dislocation density of more than 20 areas in TEM under different creep tests.

## Results and Discussion

### Starting microstructures

The metallurgical microstructures of the Al-0.7Fe and Al-0.7Fe-0.2Sc alloys in the as-cast state are shown in Figure 2. It can be clearly seen in Figure 2a that the as-cast Al-0.7Fe alloy existed with an irregular bulky shape and formed rough dendritic structure. There were a large number of intermetallic phases in the grain boundary regions, and

the average size of  $\alpha$ -Al grains is about 50  $\mu$ m. Conversely, the 0.2wt% Sc addition resulted in the better modification effect in the Al-0.7Fe-0.2Sc alloy, and the average size of  $\alpha$ -Al grains is only about 15  $\mu$ m. It is visible that the as-cast microstructure was refined efficiently. Sc addition could make grain refinement due to the formation of fine and coherent Al<sub>3</sub>Sc precipitates, which act as nucleation core [18].

Figure 3a shows the element distribution of the as-cast Al-0.7Fe-0.2Sc alloy. It can be clearly seen that Fe elements were uniformly distributed on the grain boundary, and there was a small amount of Sc elements distribution inside grain interiors. As compared with as-cast state Figures 3a and 3b, revealed a narrow grain boundary and no significant growth of grains in the annealed state. A remarkable distinction in EMPA results Figure 3, it indicates that Fe elements are present as a stable compound, with no obvious change in distribution observed after homogenization annealed. This stable compound has good thermal stability at high temperature, and it was not found to dissolve in matrix. This is consistent with the previously reported studies for Al-1Fe alloy [4]. However, the diffusion of Sc elements is from grain boundary to the matrix, as it could be expected, Sc elements uniformly dispersed in the grain interiors after homogenization annealed.

### Creep behaviors

As far as known, creeping test curves include three stages, the primary, the steady state and the accelerated creep stages, respectively. In the creeping tests, the steady state stage is the vital evaluation to creep property of materials. Figure 4 shows the creep curves of Al-0.7Fe and Al-0.7Fe-0.2Sc under different temperature of 90°C, 120°C and 150°C at 70 Mpa. This curves indicated the relationship of creeping time and strain. Listed in Table 1 are the steady state creep rates of Al-0.7Fe-0.2Sc and Al-0.7Fe under different temperatures at 70 Mpa. It can be found in Table 1 the steady state creep rate of Al-0.7Fe-0.2Sc alloy was much lower than it in Al-0.7Fe alloy. One possible reason is that the Al<sub>3</sub>Sc precipitates in the alloy during creeping process obviously impede the dislocation motions.

The steady state creep rate increased with the increasing of temperature at the same applied stress, as shown in Figure 4. To characterize the deformation mechanism of steady state creep, the value of stress exponent is the important parameter describing the relation curve between steady state creep rate and applied stress. The rate could be fitted by following equation [19]:

$$n = \left( \frac{\ln \varepsilon_s - \ln A}{\ln \sigma_0} \right)_T \quad (1)$$

Where  $\varepsilon_s$  is the steady state creep rate,  $\sigma_0$  is the applied stress,

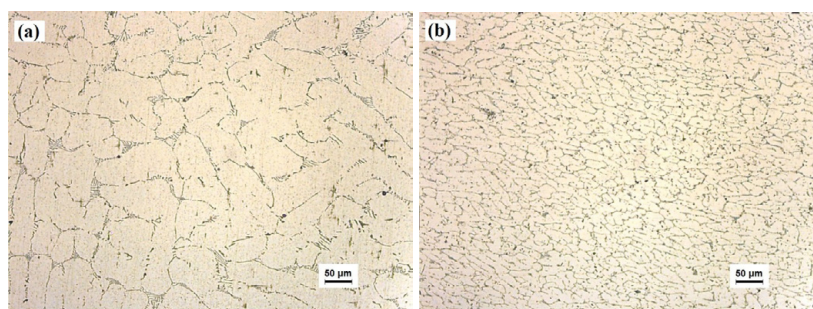


Figure 2: Optical micrographs of the as-cast state structure (a) Al-0.7 Fe (b) Al-0.7 Fe-0.2 Sc.

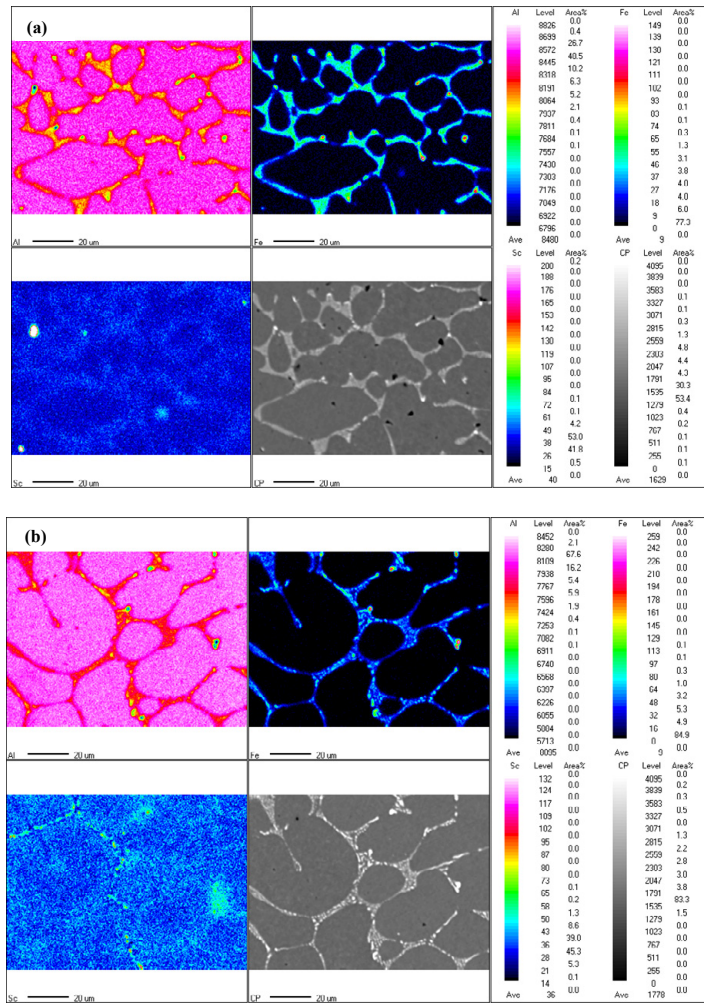


Figure 3: The EPMA elements distribution of Al-0.7 Fe-0.2 Sc alloy (a) as-cast state and (b) annealed state.

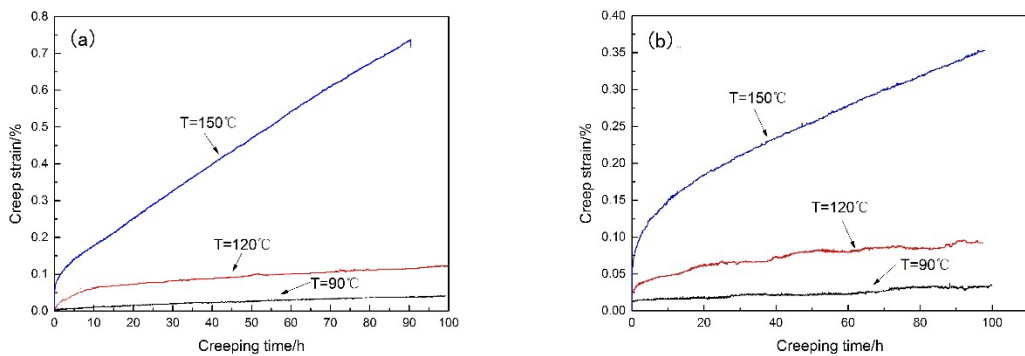


Figure 4: Al-0.7 Fe (a) and Al-0.7 Fe-0.2 Sc (b) creep curves under the temperature of 90°C, 120°C and 150°C at the stress of 70 MPa.

| Temperature (°C) | Steady state creep rate (s <sup>-1</sup> ) |                          |
|------------------|--|--------------------------|
|                  | Al-0.7 Fe                                  | Al-0.7 Fe - 0.2 Sc       |
| 90               | 2.751 × 10 <sup>-7</sup>                   | 1.203 × 10 <sup>-8</sup> |
| 120              | 9.856 × 10 <sup>-7</sup>                   | 8.674 × 10 <sup>-8</sup> |
| 150              | 2.027 × 10 <sup>-6</sup>                   | 7.346 × 10 <sup>-7</sup> |

Table 1: Steady state creep rates of the two alloys under various temperatures at 70 MPa.

A is the constant of material characteristic and the T is absolute temperature. In this work, T varies from the experiments parameters, which are constant of 363 K, 393 K and 423 K, respectively.

The value of stress exponent could be calculated by Eq. (1), and  $\sigma_0$  is the fixed value, as it can be seen in Figure 5, which presents the relation between temperature and stress exponent. It has been established that the value of stress exponent can be known the deformation mechanism of steady state creep [20]. With  $n=1$ , the creep deformation mechanism

is diffusion creep. With the range of value  $n=1-3$ , it can be judged as the dislocation slipping mechanism. With the range of value  $n=3-8$ , the dominant creep deformation mechanism is dislocation climbing, due to grain recovery at high temperature. With the value of  $n>8$ , it can be indicated that the power-law creep constitutive equation is failure. According to the present value of two alloys, the main creep deformation mechanism of Al-0.7Fe is dislocation climbing, and that of Al-0.7Fe-0.2Sc is dislocation slipping. Xu et al. [19] have found the results in his study on creep behaviors of hot-rolled Al-Cu-Mg alloy; the main creep deformation mechanism is dislocation slipping at higher applied stress.

### Microstructure after creep tests

In order to uncover the causes of the remarkably improvement on the creep-resistance property by minor Sc additions, it is indispensable to present a detailed analysis on the microstructure for the two alloys after creeping tests.

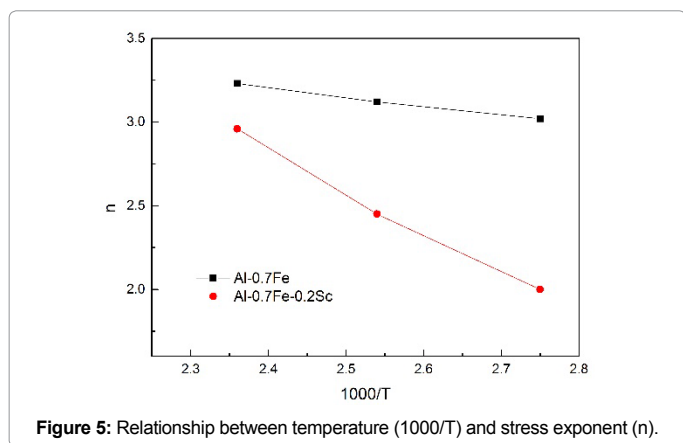


Figure 5: Relationship between temperature (1000/T) and stress exponent (n).

Figure 6 shows the TEM images of creep aged Al-0.7Fe alloy, for the purpose of comparing the creeping roles on the microstructure, three different creeping temperature specimens are also taken into consideration. As the applied stress was exerted during the creep tests, amounts of dislocations occurred near the grain boundary due to the creep strain at the stress of 70 Mpa. The bright field TEM micrographs were recorded near the  $[112]$  incident beam and the corresponding selected area diffraction (SAD) patterns were recorded to  $[112]_{Al}$  zone axes. As it can be seen from the SAD patterns, there were no detectable aging precipitates in the Al-0.7Fe alloy. The short-rod shaped phase was examined by EDX Figure 6d, it revealed a high amount of Fe in the phase and these phases were identified as  $Al_3Fe$  phases [4]. It was found that the short-rod shaped of the  $Al_3Fe$  phases are uniformly distributed along and across the grain boundaries, as a result of inhibiting the sliding the grain boundary, as shown in Figure 6a.  $Al_3Fe$  phase is thermally stable intermetallic particle [5], and it can form from the as-cast state, and once there, does not dissolve in the matrix and re-precipitate during the subsequent extrusion and heat treatments. The average size of  $Al_3Fe$  phase is  $\sim 0.4 \mu m$ , obviously, it is noted that a large number of dislocations were found in the creep sample. However, it is remarkable that the density of dislocations decreased in the sub-grain interiors, at the elevated temperature.

These locations and grain boundaries are piled up and pinned by the  $Al_3Fe$  phases, then form the wall of the dislocation. Obviously, the average size of  $Al_3Fe$  phase is  $\sim 0.4 \mu m$ ; there is no significant change in shape or size, under the temperature of 90°C, 120°C and 150°C. Considering the initial dislocation in creep aged sample is obvious Figure 6a, these dislocations should have formed after the creep deformation at the primary stage [21]. As compared with the relative high temperature creeping samples Figures 6b and 6c, the grain boundary appears to be stable during creep tests due to the appearance of triangular grain boundary, in Figure 6a. It has been investigated [22]

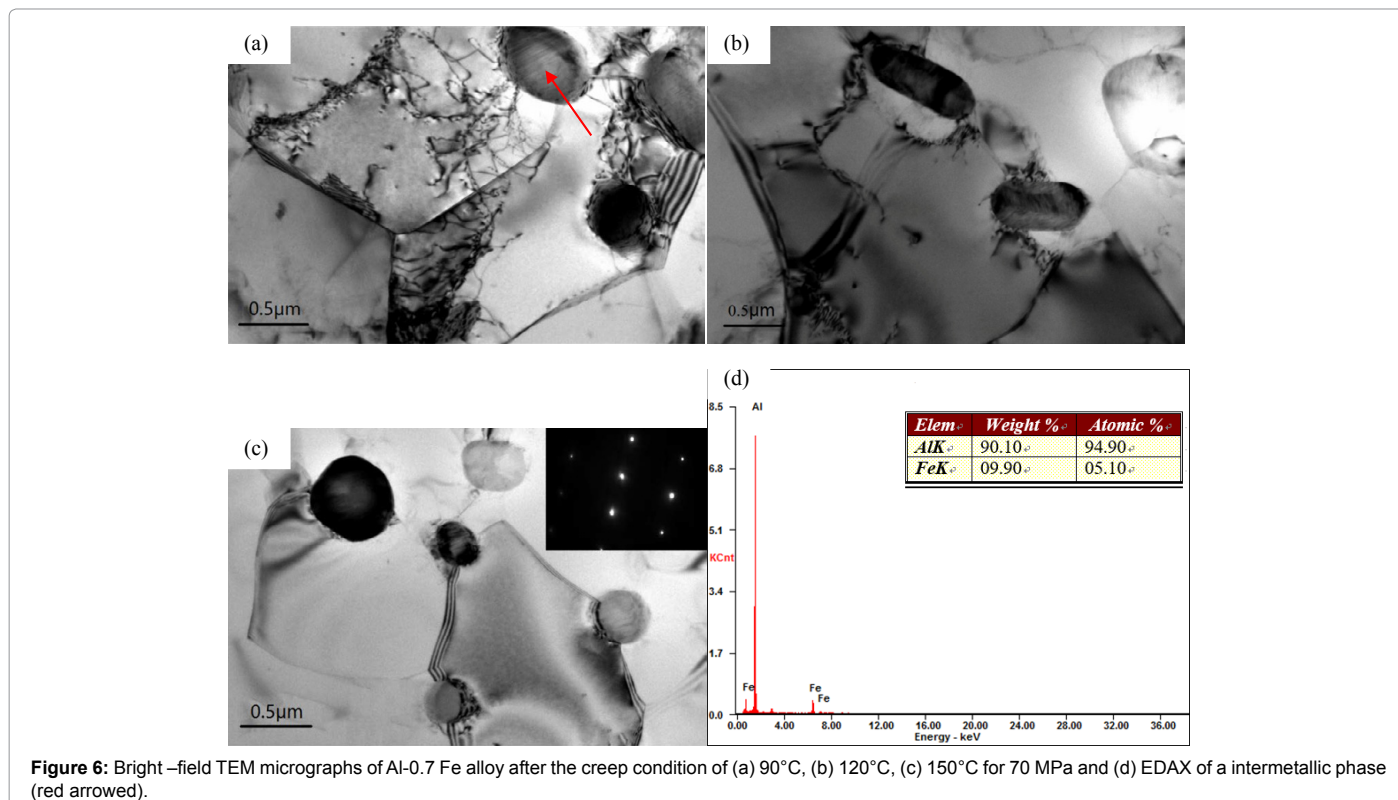
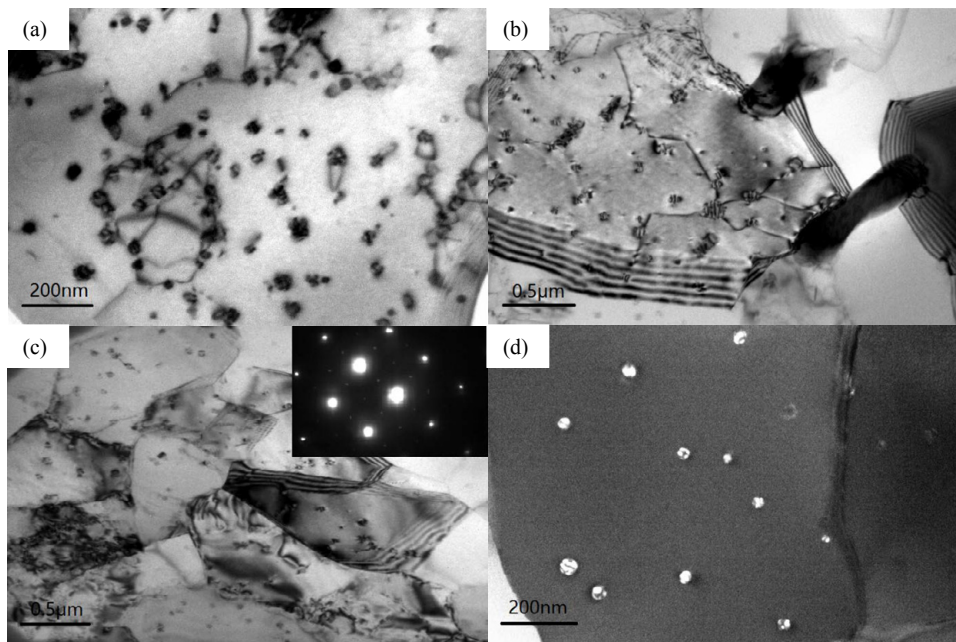


Figure 6: Bright-field TEM micrographs of Al-0.7 Fe alloy after the creep condition of (a) 90°C, (b) 120°C, (c) 150°C for 70 MPa and (d) EDAX of an intermetallic phase (red arrowed).



**Figure 7:** Bright – field TEM micrographs of Al-0.7 Fe-0.2 Sc alloy after the creep condition of (a) 90°C, (b) 120°C, (c) 150°C for 70 MPa and (d) a dark -field micrograph of creep sample.

| Temperature (°C) | Dislocation density (m <sup>-2</sup> ) |                          | Micro-hardness (HV) |                    |
|------------------|--|--------------------------|---------------------|--------------------|
|                  | Al-0.7 Fe                              | Al-0.7 Fe - 0.2 Sc       | Al-0.7 Fe - 0.2 Sc  | Al-0.7 Fe - 0.2 Sc |
| 90               | 1.1 × 10 <sup>13</sup>                 | 1.203 × 10 <sup>14</sup> | 38.7                | 45.0               |
| 120              | 9.0 × 10 <sup>11</sup>                 | 7.0 × 10 <sup>12</sup>   | 37.0                | 42.5               |
| 150              | 2.3 × 10 <sup>11</sup>                 | 4.2 × 10 <sup>12</sup>   | 32.0                | 39.8               |

**Table 2:** Dislocation density and micro-hardness of the two alloys after different creep test conditions.

that alloys with thermally stable intermetallic phase have higher creep resistance than softening intermetallic phase.

Nano sized precipitates were detected in the TEM images, as shown in Figure 7d. Superstructure peaks typical for the L1<sub>2</sub> structure could be observed from the SAD patterns, in Figure 7a. This result indicate that the creep aged precipitates are Al<sub>3</sub>Sc which were formed along with the dislocation loops and lines in the Al-0.7Fe-0.2Sc alloy, these nanosized precipitates have been identified in many researches [23,24]. In the formation of fine and coherent Al<sub>3</sub>Sc precipitates with the L1<sub>2</sub> structure, which remain high creep-resistance to ~300°C [25,26], due to a slow-diffusion element of Sc. Yu et al. [27] has found that pure Al<sub>3</sub>Sc precipitates and misfit dislocations can be observed only when the size of precipitates is larger than 16 nm. Additionally, the trace diffusivity of Sc in Al-0.7Fe alloy, may further impede the dislocations and grain boundary motions, and provide higher creep-resistance property than Al-0.7Fe alloy, as shown in Table 1. As compared with Al-0.7Fe-0.2Sc for 90°C, the even more numbers of Al<sub>3</sub>Sc phases (25 nm to 40 nm) generated along the dislocations, due to the sinks of solute and vacancies resulting in the precipitates concentration, especially for 150°C.

Figure 7a shows that an apparent number of dislocations and precipitates have emerged in the aluminum matrix, compared with the relative high temperature creeping samples Figures 7b and 7c. Whilst it is significantly weaker of dislocations pinning by Al<sub>3</sub>Sc precipitates under the temperature of 120°C and 150°C, especially for 150°C. The possible reason for this phenomenon can be attributed to the decreasing number of vacancies by the high temperature [28].

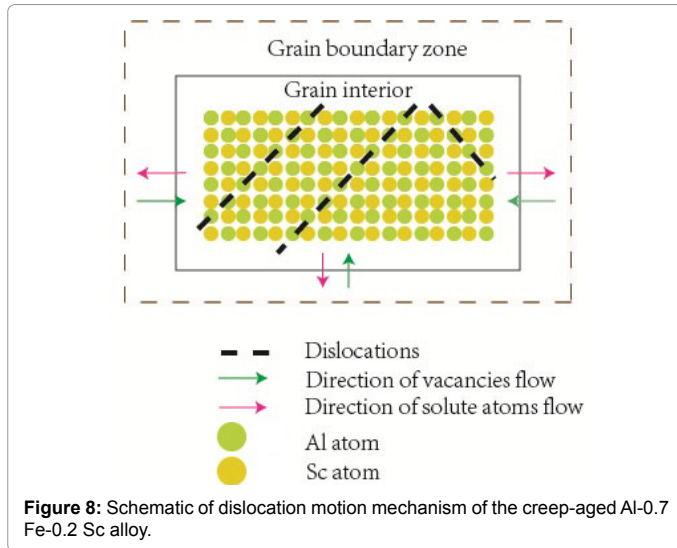
Interestingly, dislocation loops are pinned by the Al<sub>3</sub>Sc phases in the creep aged sample, as shown in Figure 7c. However, dislocation loops cannot found in the Al-0.7Fe alloy Figure 6. In addition to retard of the grain boundary motions by Al<sub>3</sub>Fe phases, the Al<sub>3</sub>Sc precipitates play an important role in interacting with dislocations. The dislocation loops have two strengthening mechanisms: the dislocation proliferation of Frank-Read and the second phase strengthening. Thus, the steady state creep rates of Al-0.7Fe-0.2Sc was smaller than that of Al-0.7Fe, this phenomenon can be attributed to the increasing numbers of dislocations and Al<sub>3</sub>Sc precipitates strengthening.

### Creep mechanism of dislocation

Creep strain is usually controlled by dislocations motions, solute matrix interaction and precipitates [29]. Moreover, formation of dislocations has three main factors: crystal growth, vacancies accumulation and stress concentration. In this work, a large quantity of vacancies formed during the homogenized treatment and hot-extrusion. Then the supersaturated vacancies accumulate after quenching and crumble to form dislocations. These dislocations are pinned by forming precipitates during the creep test. The dislocations have been proliferated due to the applied stress of crystal. The dislocation density and microhardness are showed in Table 2. As for the interaction of dislocations with thermally stable intermetallic particles, the microhardness have been improved, the microhardness for Al-0.7Fe is 38.7 HV, and that of Al-0.7Fe-0.2Sc is 45.0 HV, under the temperature of 90°C at 70 Mpa. Furthermore, the formed dislocation loops Figure 7 can be due to the vacancies condensation and sink. This suggests that this phenomenon can be explained by Orowan looping mechanism (precipitate shearing or bypass). According to the theories of dislocations, in order to force the dislocations line to bend, the required shear stress, given as follows [30]:

$$\tau_c = \frac{Gb}{l} \quad (2)$$

Where  $\tau_c$  is shear stress,  $G$ ,  $b$  and  $l$  represent shear modulus for aluminum, magnitude of Burgers vector and spacing between the



particles, respectively. Obviously, it can be seen from the equation, the smaller distance, the larger shear stress. In Figures 6 and 7, it can be seen that the spacing of  $Al_3Fe$  particles are larger than that of  $Al_3Sc$ , and dislocation loops formed during the creep test Figure 7a. Therefore, these particles interact with dislocations which produce more shear stress for  $Al_3Sc$ .

To further explore the dislocation operating mechanism, previous studies considered that the coherent precipitates based on Al-Sc-based alloys, the mechanism controlling creep-resistance of Al-Sc-based alloys is dislocation bypass of precipitates [31,32]. This mechanism applies to the increment of Orowan stress with dislocation loops, and the Orowan stress increment is approximately equal to the measured yield stress increment. The Orowan stress increment,  $\Delta\sigma_{or}$  [33], can be expressed as

$$\Delta\sigma_{or} = M \frac{0.4Gb}{\pi\lambda} \frac{\ln(\frac{2\bar{R}}{b})}{\sqrt{1-\nu}} \quad (3)$$

Where  $M$  is orientation factor for aluminum matrix [34],  $G$  is for its shear modulus [35],  $\nu$  is Poisson's ratio,  $b$  is the value of Burgers vector [35],  $\bar{R}$  is intermetallic inter-particle spacing and  $\bar{R} = \pi < R > / 4$  is the average planar particle radius [36]. In order to compare the different alloy system of Al-0.7Fe and Al-0.7Fe-0.2Sc under the temperature of 90°C at 70 Mpa, the values of  $\Delta\sigma_{or}$  are calculated: the  $\Delta\sigma_{or}$  for Al-0.7Fe is 30.1 Mpa and Al-0.7Fe-0.2Sc is 98.5 Mpa. The yield stress increment of the Al-0.7Fe is 52.7 Mpa, and that of Al-0.7Fe-0.2Sc is 62.0 Mpa by measurement of experiment. This is in accordance with Orowan strengthening mechanism that Orowan stress increment is somewhat larger than yield stress increment for Al-0.7Fe-0.2Sc. Obviously, the stress increment cannot afford dislocations to bypass the intermetallic phases, so the dislocation loops are not seen in the Figures 6b and 6c. The trend of decreasing magnitude with increasing  $\lambda$  and  $\lambda$  suggested that density of precipitates is a dominant factor in Orowan strengthening mechanism, in agreement with previous studies on Al-Sc-Yb [37] and Al-Sc-Zr [24] alloy. Marsha et al. [13] also have found the differences in volume fraction and element diffusion distance that affect the creep mechanism between alloys.

In general, the elevated temperatures strongly accelerate the diffusivity of vacancies and solute atoms. In terms of  $Al_3Fe$  phases, they were pinned along the grain boundary, and the Fe elements were uniformly distributed on the grain boundary instead of grain interior,

in Figure 3. So in the present study we are focused on Al and Sc atoms which are dominantly discussed. The thermal diffusion coefficients are  $2.22 \times 10^{-5}/K$  [38] and  $1.6 \times 10^{-5}/K$  [39] for Al and Sc atom, respectively. Obviously, the applied stress creates point defects-vacancies, moving to grain boundaries which are good sinks for vacancies and interstitial. Moreover, under vacancy existence conditions there is a competition between Al and Sc atoms for vacancies and since Al atom is faster than Sc atom, resulting in coupling of Al atoms to vacancies. It can be explained by the following schematic of dislocation motion in Figure 8. As it can be seen, a counter flux [27] of Sc solute atoms have opposite direction to vacancies, and the density of dislocations decreased as it can be seen in Figures 3 and 7. These vacancies increase at grain boundary, and a counter Sc flux increases at grain interior, as it is at elevated temperature, still to a equilibrium state. It can be assured that vacancies do not completely annihilate at grain boundary, depending on the width of grain boundary and the presence  $Al_3Fe$  phases. This decreasing number of vacancies results in the observed a small amount of dislocations, in Figures 6 and 7. As mentioned above, grain boundaries and dislocations can interact distinctly with particles ( $Al_3Fe$  and  $Al_3Sc$ ). The pinning dislocations ability and creep-resistance property of Al-0.7Fe-0.2Sc are better than those of in Al-0.7Fe alloy, due to the value of steady state creep rate and the TEM micrographs observed.

## Conclusions

The creep behaviors, microstructures and creep mechanism on Al-0.7Fe and Al-0.7Fe-0.2Sc alloys under the temperature of 90°C at 70 Mpa are investigated. The following conclusions can be summarized as follows:

(1) The trace additions of Sc have a significant effect in improving the creep-resistance property of Al-Fe alloy under the temperature of 90°C, 120°C and 150°C at 70 Mpa. However, the main creep deformation mechanism of Al-0.7Fe is dislocation climbing, and that of Al-0.7Fe-0.2Sc is dislocation slipping.

(2) The improvement in creep-resistance alloy is related to proliferating dislocations from the applied stress during the creep. The intermetallic phase  $Al_3Fe$  and  $Al_3Sc$  can inhibit the dislocation motions, especially for  $Al_3Sc$  precipitates, dislocation loops have emerged in aluminum matrix. It can be calculated by the Orowan stress increment, the  $\Delta\sigma_{or}$  value of Al-0.7Fe-0.2Sc is somewhat larger than yield stress increment; however, the Al-0.7Fe is not. It can be concluded that Orowan strengthening mechanism is the dominant strengthening mechanism in Al-Fe-Sc alloy.

(3) A counter flux solute atoms have opposite direction to vacancies, resulting in the decreasing density of dislocations. It is significantly weaken dislocations pinning by  $Al_3Sc$  precipitates at elevated temperature. This is the main reason for the low creep-resistance property of Al-0.7Fe alloy.

## Acknowledgements

The authors gratefully acknowledge the Jinbei Electric Cable Co. Ltd. for providing the necessary laboratory equipments and financial support.

## References

- Valiev RZ, Murashkin MY, Sabirov I (2014) A nanostructural design to produce high-strength Al alloys with enhanced electrical conductivity. Scr Mater 76: 13-16.
- Karabay S (2008) Influence of  $AlB_2$  compound on elimination of incoherent precipitation in artificial aging of wires drawn from redraw rod extruded from billets cast of alloy AA-6101 by vertical direct chill casting. Mater Des 29: 1364-1375.

3. IEC Standards (2007) Thermal-resistant aluminum alloy wire for overhead line conductor. Designation IEC 62004.
4. Shi ZM, Gao K, Shi YT, Wang Y (2015) Microstructure and mechanical properties of rare-earth-modified Al-1Fe binary alloys. *Mater Sci Eng A* 632: 62-71.
5. Palm M (2005) Concepts derived from phase diagram studies for the strengthening of Fe-Al-based alloys. *Intermetallics* 13: 1286-1295.
6. Dobes F, Kratochvil P (2013) The effect of Zr addition on creep of Fe-30 at. % Al alloys. *Intermetallics* 43: 142-146.
7. Vo NQ, Dunand DC, Seidman DN (2014) Improving aging and creep resistance in a dilute Al-Sc alloy by microalloying with Si, Zr and Er. *Acta Mater* 63: 73-85.
8. Harada Y, Dunand DC (2009) Microstructure of Al<sub>3</sub>Sc with ternary rare-earth additions. *Intermetallics* 17: 17-24.
9. Wu H, Wen SP, Gao KY, Huang H, Wang W, et al. (2014) Effect of Er additions of Al-Hf alloys on the precipitation strengthening. *Scr Mater* 87: 5-8.
10. Wen SP, Gao KY, Li Y, Huang H, Nie ZR (2011) Synergetic effect of Er and Zr on the precipitation hardening of Al-Er-Zr alloy. *Scr Mater* 65: 592-595.
11. Jones MJ, Humphreys FJ (2003) Interaction of recrystallization and precipitation: The effect of Al<sub>3</sub>Sc on the recrystallization behaviour of deformed aluminium. *Acta Mater* 51: 2149-2159.
12. Vlach M, Stulikova I, Smola B, Zaludova N, Cerna J (2010) Phase transformations in isochronally annealed mould-cast and cold-rolled Al-Sc-Zr-based alloy. *J Alloys Compd* 492: 143-148.
13. Van Dalen ME, Seidman DN, Dunand DC (2008) Creep and coarsening properties of Al-0.06at.%Sc-0.06at.%Ti at 300-450°C. *Acta Mater* 56: 4369-4377.
14. Gaydos DJ, Draper SL, Nathal MV (1989) Microstructure and tensile properties of Fe-40At.pct Al alloys with C, Zr, Hf, and B additions. *Metall Trans* 20: 1701-1714.
15. Van Dalen ME, Karnesky RA, Cabotaje JR, Dunand DC, Seidman DN (2009) Erbium and ytterbium solubilities and diffusivities in aluminum as determined by nanoscale characterization of precipitates. *Acta Mater* 57: 4081-4089.
16. Cubero JM, Horita Z (2015) Age hardening in ultrafine-grain Al-2pct Fe alloy processed by high-pressure torsion. *Metall Mater Trans A* 46: 2614-2624.
17. Tcherdyntsev VV, Kaloshkin SD, Gunderov DV, Afonina EA, Brodova IG, et al. (2004) Phase composition and microhardness of rapidly quenched Al-Fe alloys after high pressure torsion deformation. *Mater Sci Eng A* 375-377: 888-893.
18. Dang JZ, Huang YF, Cheng J (2009) Effect of Sc and Zr on microstructure and mechanical properties of as-cast Al-Mg-Si-Mn alloys. *Trans Nonferrous Met Soc China* 19: 540-544.
19. Xu YQ, Zhan LH, Xu LZ, Huang MH (2017) Experimental research on creep aging behaviors of Al-Cu-Mg alloy with tensile and compressive stresses. *Mater Sci Eng A* 682: 54-62.
20. Dieringa H, Hort H, Kainer KU (2009) Investigation of minimum creep rates and stress exponents calculated from tensile and compressive creep data of magnesium alloy AE42. *Mater Sci Eng A* 510-511: 382-386.
21. Xu YQ, Zhan LH, Li WK (2017) Effect of pre-strain on creep aging behavior of 2524 aluminum alloy. *J Alloy Compd* 691: 564-571.
22. Amberger D, Eisenlohr P, Goken M (2012) On the importance of a connected hard-phase skeleton for the creep resistance of Mg alloys. *Acta Mater* 60: 2277-2289.
23. Harada Y, Dunand D (2002) Microstructure of Al<sub>3</sub>Sc with ternary transition-metal additions. *Mater Sci Eng A* 329: 686-695.
24. Fuller CB, Seidman DN, Dunand DC (2003) Mechanical properties of Al(Sc,Zr) alloys at ambient and elevated temperatures. *Acta Mater* 51: 4803-4814.
25. Iwamura S, Miura Y (2004) Loss in coherency and coarsening behavior of Al<sub>3</sub>Sc precipitates. *Acta Mater* 52: 591-600.
26. Royset J, Ryum N (2005) Kinetics and mechanisms of precipitation in an Al-0.2wt.% Sc alloy. *Mater Sci Eng A* 396: 409-422.
27. Buranova Y, Kulitskiy V, Peterlechner M, Mogucheva A, Kaibyshev R, et al (2017) Al<sub>3</sub>(Sc,Zr)-based precipitates in Al-Mg alloy: Effect of severe deformation. *Acta Mater* 124: 210-224.
28. Lin YC, Xia YC, Jiang YQ, Zhou HM, Li LT (2013) Precipitation hardening of 2024-T3 aluminum alloy during creep aging. *Mater Sci Eng A* 565: 420-429.
29. Zhan LH, Lin J, Dean TA, Huang M (2011) Experimental studies and constitutive modelling of the hardening of aluminium alloy 7055 under creep age forming conditions. *Int J Mech Sci* 53: 595-605.
30. Hu GX, Cai X (2000) Materials science. Shanghai Jiaotong University, Shanghai, China.
31. Zhang JX, Harada H, Koizumi Y, Kobayashi T (2010) Dislocation motion in the early stages of high-temperature low-stress creep in a single-crystal superalloy with a small lattice misfit. *J Mater Sci*, 45(2), 523-532.
32. Rosler J, Arzt E (1990) A new model based creep equation for dispersion strengthened materials. *Acta Metal* 38: 671-683.
33. Brown, LM, Cook RH, Ham RK, Purdy GR (1973) Elastic stabilization of arrays of precipitates. *Scr Mater* 7: 815-820.
34. Martin PW (1998) Precipitation Hardening. Oxford, Butterworth-Heinemann Press.
35. Ashby M, Hugh S, David C (2013) Materials. Oxford, Butterworth-Heinemann press.
36. Ardell AJ (1985) Precipitation hardening. *Metall Trans A* 16: 2131-2165.
37. Marquis EA, Seidman DN, Dunand DC (2003) Effect of Mg addition on the creep and yield behavior of an Al-Sc alloy. *Acta Mater* 51: 4751-4760.
38. <http://www.engineeringtoolbox.com/>
39. Harada Y, Dunand D (2003) Thermal expansion of Al<sub>3</sub>Sc and Al<sub>3</sub>(Sc<sub>0.75</sub>X<sub>0.25</sub>). *Scr Mater* 48: 219-222.